Solid Freeform Fabrication 2021: Proceedings of the 32nd Annual International
Solid Freeform Fabrication Symposium – An Additive Manufacturing Conference
Reviewed Paper

INVESTIGATION ON THE PROPERTIES OF REINFORCED IN718 STRUCTURES FABRICATED USING LASER POWDER BED FUSION

B. B. Ravichander*, B. Farhang*, A. Ganesh-Ram*, M. Hanumantha*, S. Ramachandra*, Y. Shinglot*, A. Amerinatanzi*†, N. Shayesteh Moghaddam*

*Mechanical & Aerospace Engineering, University of Texas at Arlington, Arlington, TX.
†Materials Science and Engineering, University of Texas at Arlington, Arlington, TX.

Abstract

Inconel 718 (IN718) superalloy, known for its high strength and corrosion resistant behavior, is widely used in the aerospace and automotive industries. Laser power bed fusion (LPBF), one of the commonly used techniques of additive manufacturing, enables the fabrication of structures with a variety of local properties. Using the same material, components with spatially varying properties can be fabricated through applying different processing parameters. In this study, IN718 composite structures were fabricated using four types of rod reinforcements with different geometry. A different set of process parameters was used to fabricated reinforcing rods compared to that of the main part. The bonding quality at the interface between the main part and reinforcements was determined by defect analysis on the microstructure results. Also, Vickers hardness test was performed at the interface in order to examine the mechanical properties of the samples. It was found out that a similar level of densification and hardness value, slightly less than the plain sample, can be achieved using helical and arc reinforcing rods. By contrast, significantly lower density and hardness were observed for the sample reinforced by square rods compared to the plain sample.

Keywords: Laser Powder Bed Fusion, Reinforcement, IN718, Microstructure, Vickers Hardness

1. Introduction

IN718, a nickel-chromium based superalloy is widely used in the field of automobile, aeronautical and aerospace industries [1-3]. IN718 is known for its corrosion resistance behavior and thus is used in nuclear power plants, turbine blades [4, 5]. IN718 is also known for its high creep, fatigue, and strength at elevated temperatures of over 700 ˚C and thus is widely used in various industries even at difficult conditions [1, 6, 7]. Casting, forging, wrought and powder metallurgy are a few common techniques used to produce near net shaped IN718 components [8, 9]. Over the years, newer and advanced manufacturing techniques have been developed for the fabrication of IN718 and other materials. These advanced manufacturing techniques can fabricate specimens with complex geometries with higher dimensional accuracy and enhanced mechanical and microstructural properties. Additive Manufacturing (AM) is layer by layer process capable of fabricating solid parts from digital models. The advantages of AM techniques include high customizability and cost-effectiveness. Compared to conventional manufacturing processes, AM technique does not require heavy machinery such as dies, casts, molds, and forges [1, 10, 11]. During the early stages, the use of AM was limited to just prototyping till the development of various processes. Rapid prototyping, Direct digital manufacturing and Rapid tooling are some of

them. Over the last decade, the manufacturability of IN718 using AM techniques has been widely studied and developed [12-17]. Selective laser melting (SLM), Selective laser sintering (SLS) techniques which fall under the umbrella of LPBF are AM techniques [4], have the ability to produce parts with intricate geometries and high precision of metal samples. The LPBF process has the ability to highly dense parts (~99.7% [4]) by melting a layer of metal powder over and over as designed using various CAD tools. Most of the LPBF techniques use a laser source to selectively melt the powder particles based on the imported design data [18-21]. The LPBF fabricated parts seem to have acceptable microstructural and mechanical properties; however, there is still room for improvement and thus LPBF produced IN718 parts are still widely being studied [8].

The properties of LPBF IN718 has been widely studied and improved by varying the process parameters such as laser power (LP), scan speed (SS), hatch spacing (HS), layer thickness (LT), scan strategy, laser beam diameter [20, 22-24]. Jia *et al.* conducted a study by varying the LP and SS to increase the density of the parts. It was found that as the ratio between LP and SS increased, the density of the samples increased. In a similar study conducted by Ravichander *et al.* [25], it was observed that the scan speed was the significant factor in determining the grain growth of the samples and in turn the final dimension of the as-built IN718 samples. Chlebus *et al.* [26] conducted a study to increase the density of the IN718 specimens and achieved 99.8% dense parts by using double scanning strategies. The microstructural analysis of LPBF IN718 is an important one as a clear understanding of the microstructure helps us in tailoring characteristics of the specimens. Thus, Wang *et al.* conducted a study to understand the melting and the solidification process in SLM process [27]. Farhang *et al.* [28] concluded that by performing a thorough microstructural analysis, the LPBF parts could then be tailored to the desired requirements. The changes in the process parameters can lead to the formation of non-columnar grains [29]. Pröbstle *et al*. [30] studied the relation between heat transfer rate and wall thickness. It was determined that as the wall thickness varies, the heat transfer rate varies due to the changes in the rate of heat conduction. Amato *et al*. [31] investigated the correlation between process parameters and mechanical properties of IN718 samples and established that with the use of irregular process parameters, the mechanical properties of the samples deteriorated. Munaganuru *et al*. [32] performed a similar study and revealed that changes in the attributes of the samples are due to the changes in the process parameter set used. It must also be noted that the hardness values of the samples decrease as the laser power of the samples decrease [31]. The hardness of the samples increases as the density of the samples increased as mentioned by Gong *et al.* [33].

As discussed earlier, the process parameters play a significant role in establishing the different characteristics of the as-built LPBF parts. Thus, in this study a novel approach has been used to have two different process parameters and therefore leading to two different properties in a single part making it a composite structure. Cubic samples with reinforced rods of different geometries and different process parameter sets are fabricated in order to study the effect of multi-process parameters on the microstructure and hardness of the as-built samples.

2. Materials and Methods

2.1 Computer Aided Design

A total of 4 cubic parts, each having a dimension of 10 mm x 10 mm x 5 mm, were modeled with the help of Solidworks (version 2018-2019, Dassault Systems, USA). To investigate the effect of different rod geometry, four different rod geometries (plain rods, helical rods, arc rods and square rods) were designed. The helical, arc and square rods are the additional geometries added to the plain rod as shown in figure 1.

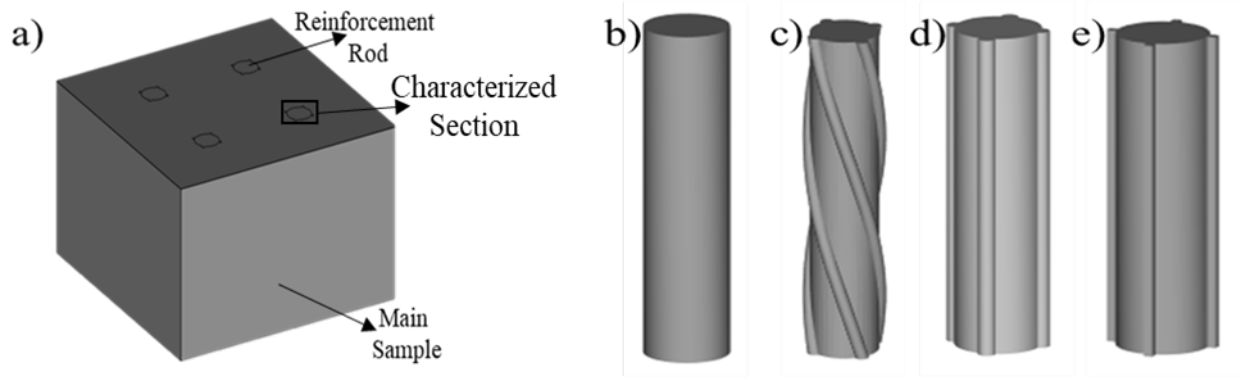

Figure 1. Computer-aided designs of the four different rod geometries: a) main part reinforced with rods, b) plain rod, c) helical rod, d) arc rod and e) square rod. Reinforced rods shown in figures b-e have been fabricated using a set of process parameter different from that used for the main sample.

2.2 Powder Preparation and Fabrication

The IN718 powder was obtained from EOS (EOS GmbH, Electro Optical Systems, Germany). The composition of the as-obtained powder was determined using Energy-dispersive X-ray spectroscopy (EDS) analysis is as shown in table 1 and the scanning electron microscope (SEM) micrograph of the fresh powder is as shown in figure 2a. The analysis of the SEM micrograph of the fresh powder revealed the average powder particle size to be 12 microns. ImageJ [34], a license-free software was used to analyze the particle size and with the help of those results, and a histogram of the particle-size distribution was generated, as shown in Figure 2b.

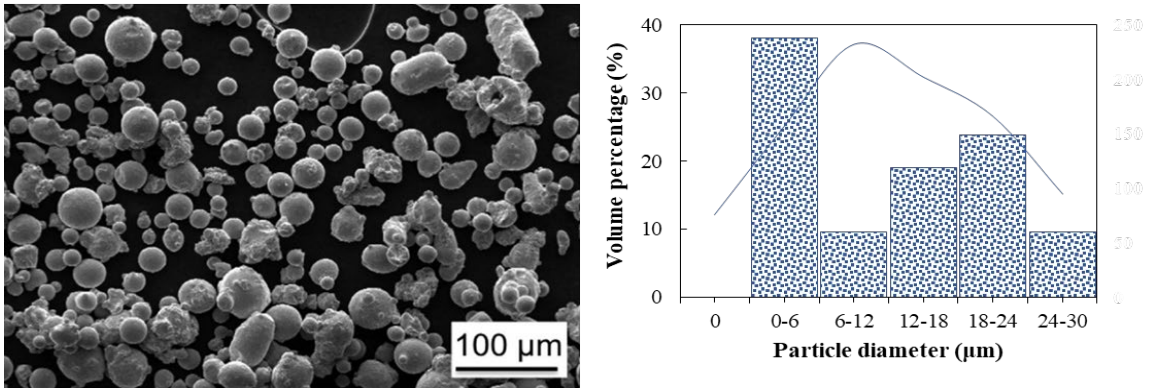

Figure 2. (a) SEM micrograph of powder; (b) particle size distribution for commercial EOS IN 718 powder

Table 1. The chemical composition of IN718 powder obtained from EOS

Element	Ni	Cr	Nb	Mo	Ti	Al	Fe
Wt%	50-55	17-21	4.75-5.5	2.8-3.3	0.65-1.15	0.2-0.8	Balance

An EOS M290 laser powder-bed fusion process printer equipped with a 400 W Ytterbium fiber laser was used in the fabrication of the IN718 samples. The process chamber was purged with Argon gas to reduce oxidation due to atmospheric oxygen and the build plate was heated to 80 °C. Except for the laser power, same process parameters used for the fabrication of the main sample and reinforced rods. 110 µm hatching distance, 40 µm layer thickness, 100 µm laser beam diameter, and 960 mm/s scanning speed with stripes scan strategy (having a hatch angle of 67°) were applied during the fabrication process. Table 2 shows the laser power and energy density of the components of the samples. The energy density was calculated with the help of the following equation [35-37]:

$$E_d = \frac{LP}{SS * HS * LT}$$

Where E_d (J/mm^3) is energy input, LP (W) is laser power, SS (mm/s) is scanning speed, HS (µm) is hatch distance, and LT (µm) is layer thickness.

Table 2. The laser power and energy density of the samples' components

Component of the sample	Laser Power (W)	Energy Density (J/mm^3)
Main part	285	67.7
Reinforced rods	256.5	60.7

2.3 Experimental Procedure

The microstructural analysis of the as-built IN718 parts was carried out using a Hitachi S-3000N Variable Pressure SEM. To perform microstructure characterization, the samples were cold-mounted using epoxy resins. Once the resin hardened, the samples were ground and polished using an Allied E- prep 4™ (Allied High-Tech Products, Inc., Compton, CA). Silicon Carbide (SiC) abrasive discs were used to carry out grinding and this was done till a uniform scratch pattern was obtained. After grinding, two polishing steps were conducted in order to remove the deformation caused due to grinding. This was done using a 1 µm diamond suspension on DiaMat polishing cloth and the final step was performed with 0.05 µm colloidal silica suspension on a Red Final C polishing cloth. The Vickers hardness of the samples was determined with the help of a Leco LM 300 AT microhardness tester under an applied load of 500 g for 10 seconds, where 4 indentations were performed on each specimen to declare the average hardness value.

3. Results and Discussion

3.1 Microstructural Analysis

Defect formation analysis of the as-built samples was conducted in order to study the cohesive behavior between the main sample and the reinforced rod. Figure 3 shows the cracks observed at the interface of the main sample and its reinforced rod. From figure 3, it is evident that there are cracks and surface porosities at the interface. ImageJ software was used to determine the percentage of porosity for four sections at the interface and their values have been plotted in figure 4. From figures 3a and figure 4, it is clear that the plain rod sample had the least amount of surface porosity of 2.6% among all the samples. This observation can be expected as the plain sample was fabricated homogenously without having an interface with any strengthening segment. In terms of samples fabricated with reinforcements, the samples fabricated with helical and arc rods had a surface porosity of 2.8% and 3.2%, respectively, as can be seen in figure 4. The similar level of surface porosity observed for these samples can be attributed to the similar cross-section of their interface with the main section. Although the interface geometry for the sample reinforced by the helical rods varies along with the height, it makes a circular interface geometry in each cross-section. Therefore, focusing on a cross-section at a specific height, similar results are expected for samples fabricated with arc and helical reinforcements. Moreover, it is clear from figure 4 that the sample fabricated with square rods had the highest porosity percentage of 8.5%. This can be attributed to the higher stress concentration arising from the sharp angles exist in the geometry of square rods. As the local stress concentration increases, the probability of initiation and formation of cracks increases [38]. This is consistent with the highest level of porosities was found for the sample reinforced by square rods with the highest stress concentration in the interface.

In terms of size of the defects (figure 4), the average value was similar for the samples reinforced by plain and helical rod (8.42 and 8.32 micron respectively), but it increased for the sample with arc rod (9.27 micron). As expected, the average defect size was highest for the sample reinforced by the square rod (10.45 micron) that can be again attributed to the high level of stress concentration. It has been revealed that besides the porosity level, size of defects plays a significant role in the fatigue life of the LPBF processed parts [39]. Generally, formation of defects with irregular shape and large size results in high stress concentration and thereby lower fatigue strength [40, 41]. Although analyzing the morphology of the defects showed formation of irregular shaped pores for all the samples, the size of the defects varied among the reinforced parts. According to the results, a lower tensile strength and fatigue life is expected for the sample with square rods due to the formation of larger defects in this sample.

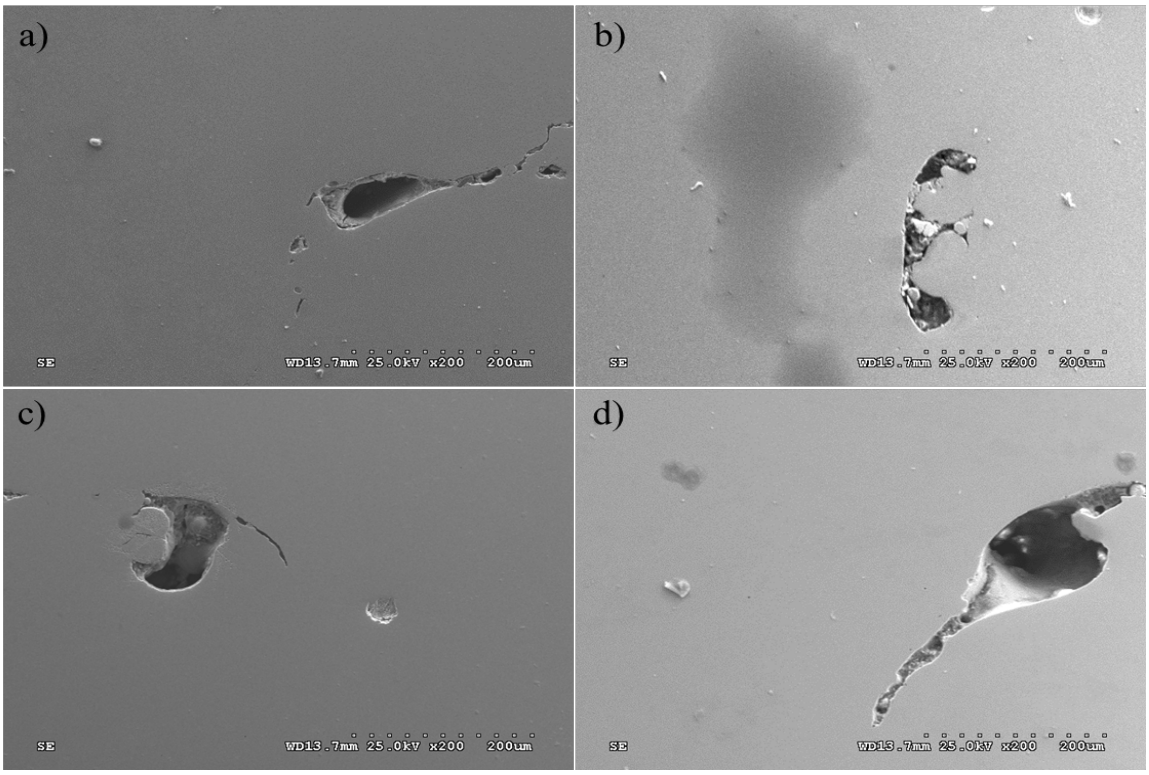

Figure 3. SEM micrographs showcasing the porosities at the interface between the main part and the reinforcement. a) plain rod, b) helical rod, c) arc rod and d) square rod.

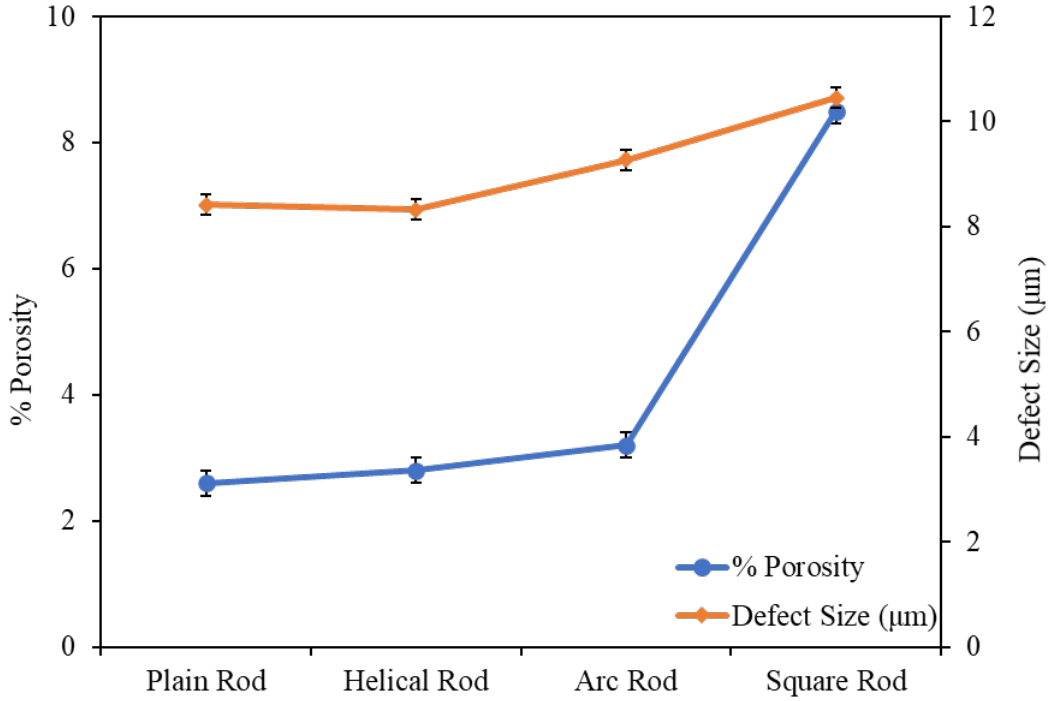

Figure 4. Percentage of surface porosities at the interface between the reinforced rods and the main sample for the four samples. Higher surface porosities were seen for the samples fabricated with square rod and arc rods.

3.2 Hardness Analysis

The Vickers hardness values measured at the interface between the main samples and the reinforced rods are shown in figure 5. The sample fabricated with plain rods as reinforcement resulted in higher Vickers hardness of 295.11 HV at the interface. The samples fabricated with helical rods and arc rods as interface had average Vickers hardness values of 260.84 HV and 257.27 HV, respectively. However, the sample fabricated with the square rod as reinforcement yielded a low hardness value of 212.79 HV. It has been revealed that there is an inverse relation between the level and the size of defects and the microhardness value [42]. As discussed in section 3.1, the highest and lowest levels of surface porosity was found for the sample reinforced by square rods and the plain sample, respectively. Therefore, it is reasonable to see lowest and highest hardness value for the former and latter, respectively. Also, it is expected to observe similar hardness value for the samples reinforced by helical and arc rods, as they showed a similar level of surface porosity at the interface of the main sample and the reinforced rods.

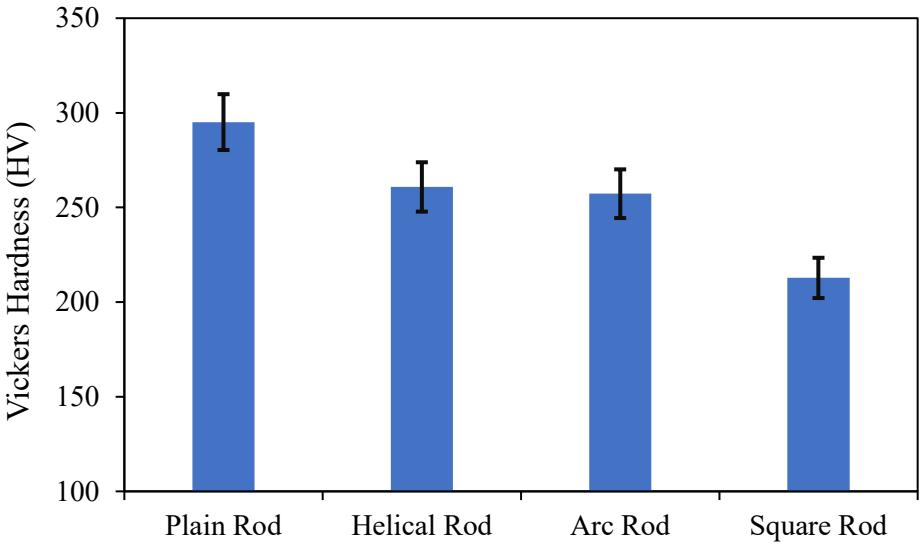

Figure 5. The average Vickers hardness values for the four samples were obtained at the interface between the reinforced rods and the main sample. Higher average Vickers hardness was seen in the samples fabricated with the plain rods, while the lowest value was observed at the interface in the sample fabricated with the square rods as reinforcements.

4. Conclusion

In this study, cubic samples with reinforced rods of different geometries and process parameters are fabricated. The effect of these reinforced rods on the microstructure and Vickers hardness values are studied. It was found that the plain rod reinforcements had lower levels of surface porosity compared to the other samples. The Helical and the Arc rods are similar in terms of cross section and had similar levels of surface porosities. The square rods, however, had a high percentage of surface porosity due to the sharp edges. The Vickers hardness analysis of the samples at the interface between the rods and the main sample revealed that the plain rod sample had the highest hardness value and the samples fabricated with the square rod resulted in the lowest Vickers hardness value.

5. Acknowledgement

This work was supported by a University of Texas System STARs award.

6. References

1. Calandri, M., et al., *Texture and Microstructural Features at Different Length Scales in Inconel 718 Produced by Selective Laser Melting.* Materials, 2019. **12**(8): p. 1293.
2. Beaman, J.J., et al., *Solid Freeform Fabrication: A New Direction in Manufacturing*. Vol. 1. 1997: Springer US. IX, 330.
3. Chua, C.K., K.F. Leong, and C.S. Lim, *Rapid Prototyping, Principles and Applications.* Assembly Automation, 2010. **30**(4).
4. Mostafa, A., et al., *Structure, Texture and Phases in 3D Printed IN718 Alloy Subjected to Homogenization and HIP Treatments.* Metals, 2017. **7**(6).
5. Amato, K.N., et al., *Microstructures and mechanical behavior of Inconel 718 fabricated by selective laser melting.* Acta Materialia, 2012. **60**(5): p. 2229-2239.
6. Thomas, A., et al., *High Temperature Deformation of Inconel 718.* Journal of Materials Processing Technology, 2006. **177**: p. 469-472.
7. Pieraggi, B. and J.-F. Uginet. *Fatigue and creep properties in relation with alloy 718 microstructure* 1998.
8. Holland, S., et al., *Multiscale characterization of microstructures and mechanical properties of Inconel 718 fabricated by selective laser melting.* Journal of Alloys and Compounds, 2019. **784**: p. 182-194.
9. Popovich, V.A., et al. *Creep and Thermomechanical Fatigue of Functionally Graded Inconel 718 Produced by Additive Manufacturing*. 2018. Cham: Springer International Publishing.
10. DebRoy, T., et al., *Additive manufacturing of metallic components – Process, structure and properties.* Progress in Materials Science, 2018. **92**: p. 112-224.
11. Murr, L.E., et al., *Fabrication of Metal and Alloy Components by Additive Manufacturing: Examples of 3D Materials Science.* Journal of Materials Research and Technology, 2012. **1**(1): p. 42-54.
12. Murr, L.E., *Metallurgy of additive manufacturing: Examples from electron beam melting.* Additive Manufacturing, 2015. **5**: p. 40-53.
13. Jia, Q. and D. Gu, *Selective laser melting additive manufacturing of Inconel 718 superalloy parts: Densification, microstructure and properties.* Journal of Alloys and Compounds, 2014. **585**: p. 713-721.
14. Kuo, Y.-L., S. Horikawa, and K. Kakehi, *The effect of interdendritic δ phase on the mechanical properties of Alloy 718 built up by additive manufacturing.* Materials & Design, 2017. **116**: p. 411-418.
15. Gong, X. and K. Chou. *Microstructures of Inconel 718 by Selective Laser Melting*. 2016. Cham: Springer International Publishing.
16. Murr, L.E., et al., *Microstructural Architecture, Microstructures, and Mechanical Properties for a Nickel-Base Superalloy Fabricated by Electron Beam Melting.* Metallurgical and Materials Transactions A, 2011. **42**(11): p. 3491-3508.
17. Wang, Z., et al., *The microstructure and mechanical properties of deposited-IN718 by selective laser melting.* Journal of alloys and compounds, 2012. **513**: p. 518-523.

18. Yan, C., et al., *Evaluations of cellular lattice structures manufactured using selective laser melting.* International Journal of Machine Tools and Manufacture, 2012. **62**: p. 32-38.
19. Gebhardt, A., et al., *Additive Manufacturing by selective laser melting the realizer desktop machine and its application for the dental industry.* Physics Procedia, 2010. **5**: p. 543-549.
20. Qi, H., M. Azer, and A. Ritter, *Studies of Standard Heat Treatment Effects on Microstructure and Mechanical Properties of Laser Net Shape Manufactured INCONEL 718.* Metallurgical and Materials Transactions A, 2009. **40**(10): p. 2410-2422.
21. Maamoun, A.H., et al., *The Effect of Selective Laser Melting Process Parameters on the Microstructure and Mechanical Properties of Al6061 and AlSi10Mg Alloys.* Materials, 2019. **12**(1): p. 12.
22. Valdez, M., et al., *Induced porosity in Super Alloy 718 through the laser additive manufacturing process: Microstructure and mechanical properties.* Journal of Alloys and Compounds, 2017. **725**: p. 757-764.
23. Ni, M., et al., *Anisotropic tensile behavior of in situ precipitation strengthened Inconel 718 fabricated by additive manufacturing.* Materials Science and Engineering: A, 2017. **701**: p. 344-351.
24. Ravichander, B.B., et al., *A Prediction Model for Additive Manufacturing of Inconel 718 Superalloy.* Applied Sciences, 2021. **11**(17).
25. Ravichander, B.B., A. Amerinatanzi, and N. Shayesteh Moghaddam, *Study on the Effect of Powder-Bed Fusion Process Parameters on the Quality of as-Built IN718 Parts Using Response Surface Methodology.* Metals, 2020. **10**(9).
26. Chlebus, E., et al., *Effect of heat treatment on the microstructure and mechanical properties of Inconel 718 processed by selective laser melting.* Materials Science and Engineering: A, 2015. **639**: p. 647-655.
27. Wang, Z., et al., *The microstructure and mechanical properties of deposited-IN718 by selective laser melting.* Journal of Alloys and Compunds, 2012. **513**: p. 6.
28. Farhang, B., et al., *Study on variations of microstructure and metallurgical properties in various heat-affected zones of SLM fabricated Nickel-Titanium alloy.* Materials Science and Engineering: A, 2020. **774**.
29. Brenne, F., et al., *Microstructural design of Ni-base alloys for high-temperature applications: impact of heat treatment on microstructure and mechanical properties after selective laser melting.* Progress in Additive Manufacturing, 2016.
30. Pröbstle, M., et al., *Superior creep strength of a nickel-based superalloy produced by selective laser melting.* Materials Science and Engineering: A, 2016. **674**.
31. Amato, K.N., et al., *Microstructures and mechanical behavior of Inconel 718 fabricated by selective laser melting.* Acta Materialia, 2012. **60**(5).
32. Munaganuru, S.S.N.E., Muthu Ram Prabhu & Vadlamudi, Vamsee & Shaik, Rauhon Ahmed & Adluru, Hari Kishore & Raihan, Md Rassel & Reifsnider, Kenneth. , *Effects of Build Parameters on the Mechanical and Di-Electrical Properties of AM parts.* (2018).
33. Gong, X., et al., *Characterization of Microstructure and Mechanical Property of Inconel 718 from Selective Laser Melting*, in *ASME 2015 International Manufacturing Science and Engineering Conference*. 2015: Charlotte, North Carolina.
34. Rasband, W., *ImageJ*. National Institutes of Health and the Laboratory for Optical and Computational Instrumentation: Wisconsin.
35. Bharath Bhushan, R., A. Amirhesam, and M. Narges Shayesteh. *Toward mitigating microcracks using nanopowders in laser powder bed fusion*. in *Proc.SPIE*. 2021.

36. Bharath Bhushan, R., et al. *Analysis of the deviation in properties of selective laser melted samples fabricated by varying process parameters*. in *Proc.SPIE*. 2020.
37. Bharath Bhushan, R., et al. *A framework for the optimization of powder-bed fusion process*. in *Proc.SPIE*. 2021.
38. Farhang, B., et al., *Study on variations of microstructure and metallurgical properties in various heat-affected zones of SLM fabricated Nickel–Titanium alloy.* Materials Science and Engineering: A, 2020. **774**: p. 138919.
39. Zhang, B., Y. Li, and Q. Bai, *Defect Formation Mechanisms in Selective Laser Melting: A Review.* Chinese Journal of Mechanical Engineering, 2017. **30**(3): p. 515-527.
40. Gong, H., et al., *Influence of defects on mechanical properties of Ti–6Al–4V components produced by selective laser melting and electron beam melting.* Materials & Design, 2015. **86**: p. 545-554.
41. Liu, Q., et al., *The Effect of Manufacturing Defects on The Fatigue Behaviour of Ti-6Al-4V Specimens Fabricated Using Selective Laser Melting.* Advanced Materials Research, 2014. **891-892**: p. 1519-1524.
42. Tucho, W.M., et al., *Investigation of effects of process parameters on microstructure and hardness of SLM manufactured SS316L.* Journal of Alloys and Compounds, 2018. **740**: p. 910-925.